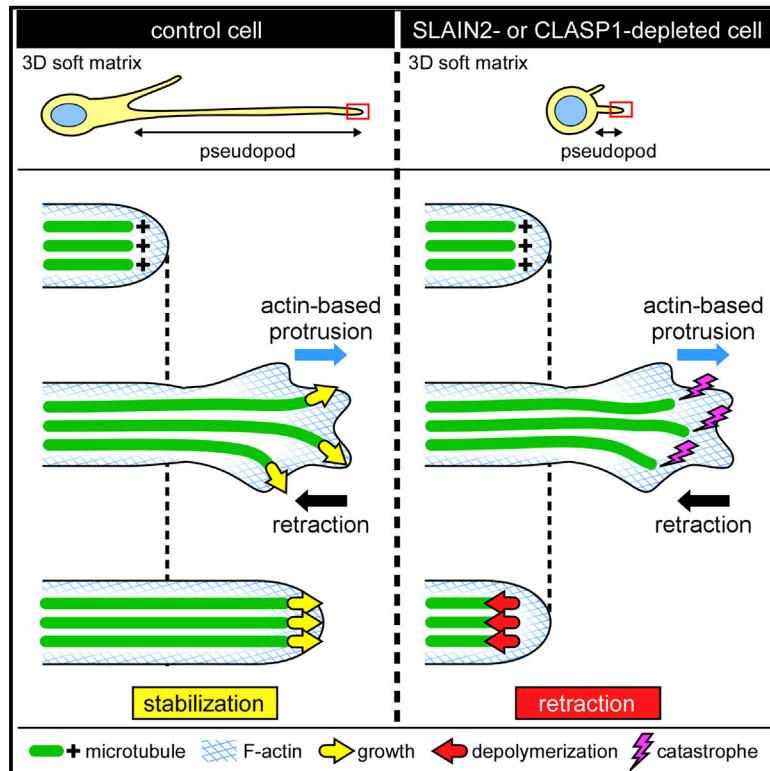


# Developmental Cell

## Mesenchymal Cell Invasion Requires Cooperative Regulation of Persistent Microtubule Growth by SLAIN2 and CLASP1

### Graphical Abstract



### Authors

Benjamin P. Bouchet, Ivar Noordstra, Miranda van Amersfoort, ..., Marileen Dogterom, Patrick W.B. Derksen, Anna Akhmanova

### Correspondence

bouchetben@gmail.com (B.P.B.), a.akhmanova@uu.nl (A.A.)

### In Brief

Bouchet, Noordstra et al. identify microtubule plus-end tracking proteins (+TIPs) SLAIN2 and CLASP1 as essential regulators of mesenchymal cell morphogenesis and migration in soft 3D matrices. Persistent microtubule growth supports cell elongation in 3D, and its attenuation in interphase is a potent strategy to inhibit tumor invasion and metastasis.

### Highlights

- Mesenchymal cell migration in 3D depends on persistent microtubule growth
- SLAIN2 and CLASP1 suppress cortical catastrophes and promote cell elongation
- Inhibition of microtubule depolymerization is sufficient for pseudopod maintenance
- Attenuation of microtubule growth persistence in interphase suppresses tumor invasion



# Mesenchymal Cell Invasion Requires Cooperative Regulation of Persistent Microtubule Growth by SLAIN2 and CLASP1

Benjamin P. Bouchet,<sup>1,5,\*</sup> Ivar Noordstra,<sup>1,5</sup> Miranda van Amersfoort,<sup>2</sup> Eugene A. Katrukha,<sup>1</sup> York-Christoph Ammon,<sup>1</sup> Natalie D. ter Hoeve,<sup>2</sup> Louis Hodgson,<sup>3</sup> Marileen Dogterom,<sup>4</sup> Patrick W.B. Derksen,<sup>2</sup> and Anna Akhmanova<sup>1,6,\*</sup>

<sup>1</sup>Cell Biology, Department of Biology, Faculty of Science, Utrecht University, Padualaan 8, 3584 CH Utrecht, the Netherlands

<sup>2</sup>Department of Pathology, University Medical Center Utrecht, Heidelberglaan 100, 3584 CX Utrecht, the Netherlands

<sup>3</sup>Department of Anatomy and Structural Biology, Gruss-Lipper Biophotonics Center, Albert Einstein College of Medicine, Bronx, NY 10461, USA

<sup>4</sup>Department of Bionanoscience, Kavli Institute of Nanoscience, Delft University of Technology, Lorentzweg 1, 2628 CJ Delft, the Netherlands

<sup>5</sup>Co-first author

<sup>6</sup>Lead Contact

\*Correspondence: [bouchetben@gmail.com](mailto:bouchetben@gmail.com) (B.P.B.), [a.akhmanova@uu.nl](mailto:a.akhmanova@uu.nl) (A.A.)

<http://dx.doi.org/10.1016/j.devcel.2016.11.009>

## SUMMARY

Microtubules regulate signaling, trafficking, and cell mechanics, but the respective contribution of these functions to cell morphogenesis and migration in 3D matrices is unclear. Here, we report that the microtubule plus-end tracking protein (+TIP) SLAIN2, which suppresses catastrophes, is not required for 2D cell migration but is essential for mesenchymal cell invasion in 3D culture and in a mouse cancer model. We show that SLAIN2 inactivation does not affect Rho GTPase activity, trafficking, and focal adhesion formation. However, SLAIN2-dependent catastrophe inhibition determines microtubule resistance to compression and pseudopod elongation. Another +TIP, CLASP1, is also needed to form invasive pseudopods because it prevents catastrophes specifically at their tips. When microtubule growth persistence is reduced, inhibition of depolymerization is sufficient for pseudopod maintenance but not remodeling. We propose that catastrophe inhibition by SLAIN2 and CLASP1 supports mesenchymal cell shape in soft 3D matrices by enabling microtubules to perform a load-bearing function.

## INTRODUCTION

The ability to move through a three-dimensional (3D) matrix is a physiological feature found in many differentiated cell types and in developmental precursors (Friedl and Gilmour, 2009; Lam and Huttenlocher, 2013; Nakaya and Sheng, 2008). Besides its role in tissue morphogenesis and immune surveillance, cell invasion is also associated with metastasis in solid cancers (Chaffer and Weinberg, 2011). Importantly, cell migration modes in 3D matrices are determined by cell shape characteristics (Friedl and Gilmour, 2009). In particular, mesenchymal cell motility, found in fibroblasts, endothelial cells, embryonic cells

undergoing epithelial-mesenchymal transition (EMT), and invasive tumors, requires formation of long pseudopods (Cheung et al., 2013; Clark and Vignjevic, 2015; Friedl and Gilmour, 2009; Grinnell and Petroll, 2010; Petrie and Yamada, 2015).

The importance of microtubules (MTs) for mesenchymal pseudopod elongation in soft matrices has been known since the 1980s (Grinnell et al., 2003; Tomasek and Hay, 1984). Numerous studies showed that the destruction or perturbation of the MT network by MT-targeting agents (MTAs) abolishes pseudopod-based invasion (Kikuchi and Takahashi, 2008; Lee et al., 2015; Martins and Kolega, 2012; Oyanagi et al., 2012; Pourroy et al., 2006; Rhee et al., 2007; Tran et al., 2009). However, the molecular mechanisms responsible for the ability of MTs to support mesenchymal cell protrusions in soft matrices are yet to be established.

Until now, the mechanical involvement of the cytoskeleton in cell invasion was mostly linked to actin and its regulators (Kikuchi and Takahashi, 2008; Kutys and Yamada, 2014; Sahai and Marshall, 2003; Sanz-Moreno and Marshall, 2010; Wilson et al., 2013). In contrast, MTs are viewed as signaling and trafficking platforms that modulate cell shape by indirectly regulating Rho guanosine triphosphatases (GTPases), substrate adhesion, and polarity (Etienne-Manneville, 2013; Gierke and Wittmann, 2012; Petrie and Yamada, 2015; Rhee et al., 2007). Depletion of the plus-end tracking protein (+TIP) EB1 caused invasion defects in hepatocyte growth factor-stimulated canine epithelial cells (Gierke and Wittmann, 2012). EB1 controls the recruitment of a broad variety of other +TIPs involved in MT polymerization and depolymerization, their interaction with various cellular structures, transport, and signaling (Akhmanova and Steinmetz, 2015). The mechanistic basis for the involvement of EB1 in pseudopod protrusion thus needs to be elucidated.

Several studies introduced the idea that MTs can mechanically contribute to cell morphogenesis (Brangwynne et al., 2006; Dennerl et al., 1988; Fygenson et al., 1997a; Matrone et al., 2010; Wang et al., 2001; Winckler and Solomon, 1991). The tensegrity model suggests that the ability of MTs to withstand compression at the cell cortex controls cell shape in soft 3D matrices (Ingber, 2003). However, a limitation to such a function is that the dynamic MT tips in proximity of the cell cortex are expected to

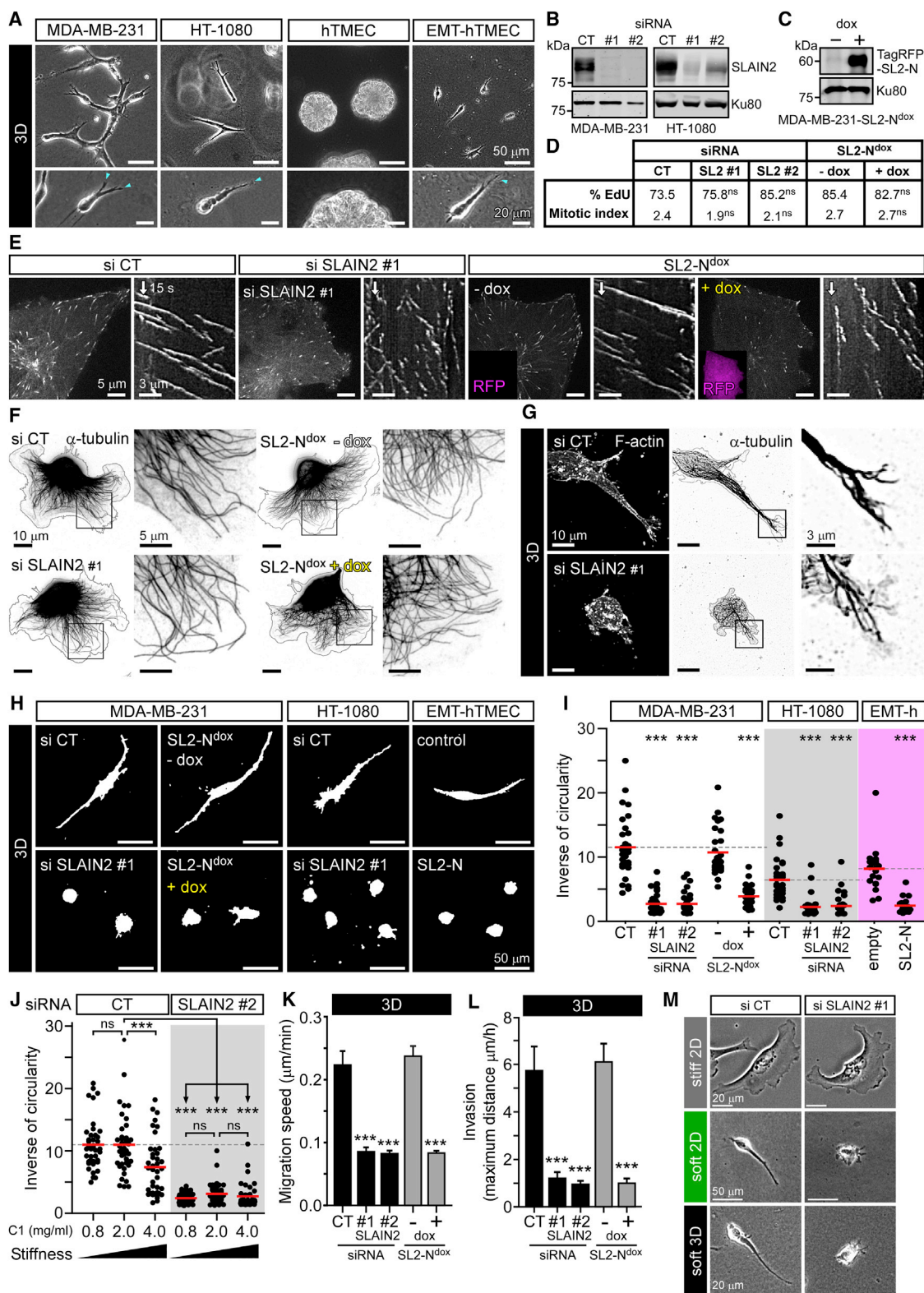


**Figure 1. SLAIN2 Is Required for Mesenchymal Cell Invasion**

(A) Morphology of cancer and non-cancer mesenchymal cells grown in collagen I-based 3D matrices. MDA-MB-231, HT-1080, and untransformed human mammary epithelial cells converted to mesenchymal cells by EMT (EMT-hTMEC, 4 days in 3D, compared with control cells hTMEC, 16 days in 3D); blue arrowheads indicate invasive pseudopods at the leading edge.

(legend continued on next page)

undergo force-induced catastrophes (Janson et al., 2003; Laan et al., 2008). An important question is thus whether physiological mechanisms of catastrophe regulation are compatible with a load-bearing function of MTs in 3D cell morphogenesis.

Here, we identify the +TIP and catastrophe inhibitor SLAIN2 (van der Vaart et al., 2011) as an essential factor for mesenchymal cell invasion both in vitro and in a mouse tumor model. This function is independent of the regulation of Rho GTPase activity, vesicle transport, and focal adhesion formation but rather underlies the resistance of dynamic MT plus ends to compression. We show that SLAIN2, as well as another +TIP, CLASP1, enable mesenchymal cells to form long invasive pseudopods by promoting highly persistent MT growth at their tips. When persistent MT growth is perturbed, suppression of MT depolymerization is sufficient for the maintenance but not for the remodeling of invasive pseudopods. Based on experimental data and computer simulations, we discuss the implications of these findings for the mechanical role of dynamic MTs in cell invasion and their relevance in cancer therapeutics.

## RESULTS

### SLAIN2-Dependent Inhibition of MT Catastrophes Is Required for Mesenchymal Cell Invasion

To test how the regulation of MT growth affects mesenchymal cell invasion, we used cancer cells from different origins (MDA-MB-231, HT-1080) and non-tumor human mammary cells carrying an inducible EMT system based on doxycycline-controlled expression of ZEB1 (Zhang et al., 2015) (Figures S1A and S1B). These three cell models displayed invasive properties when grown in a soft collagen I-based 3D matrix with characteristic long invasive pseudopods at their leading edge (Figure 1A). We previously showed that the +TIP SLAIN2 inhibits MT catastrophes specifically in interphase cells by promoting EB1-dependent recruitment of the polymerase ch-TOG to MT plus ends (van der Vaart et al., 2011). To test the importance of this mechanism for cell invasion, we inactivated SLAIN2 by RNA-interference-mediated knockdown or expression of a dominant negative mutant, SLAIN2-N (SL2-N), which binds ch-TOG but not to EB1 (Figures 1B and 1C) (van der Vaart et al., 2011). As we showed before, these treatments induced a loss of ch-TOG from MT plus ends (Figure S1C) and reduced MT growth rate and persistence (Figures S1D and S1E; Movie S1). A similar MT growth defect was observed by depleting ch-TOG (Figures

S1D–S1F), confirming the notion that the effect of SLAIN2 depletion on MT dynamics is due to the reduction of ch-TOG localization at MT plus ends. Loss of SLAIN2 function did not affect cell-cycle progression or localization of other +TIPs, such as CLIP-170 and CLASP1, to MT plus ends (Figures 1D and S1G). Although MTs showed highly interrupted growth, they still formed a morphologically normal network, the density of which was similar to control cells at the leading edge (Figures 1E, 1F, and S1H).

SLAIN2-depleted cells spread and migrated normally on a stiff 2D matrix consisting of collagen I-coated coverslips (Figures 1F, S2A, and S2B; Movie S2). However, inside soft collagen I gels (2 mg/mL), loss of SLAIN2 function caused a dramatic change in cell morphology, as the cells completely failed to form long invasive pseudopods (Figures 1G–1I and Movie S2). This defect was due to the inability of SLAIN2-depleted cells to elongate their protrusions, while protrusion initiation was unaffected (Figures S2C and S2D). Importantly, the difference between the effect of SLAIN2 depletion in 2D and 3D was not associated with the differential subcellular localization of SLAIN2, as it tracked all growing MT plus ends both on stiff 2D and in soft 3D matrices (Figure S1I). Consistently, the extent of MT dynamics perturbation by SLAIN2 inactivation was the same in soft 3D gels as on stiff 2D substrates, and MTs penetrated pseudopod tips in a similar fashion in control and SLAIN2-depleted cells (Figures S1D, S1E, and 1G).

Matrix stiffness can influence MT stability and their ability to activate Rho to control cell contractility (Heck et al., 2012). Based on previous studies, we defined collagen I concentration ranging from 0.8 to 4 mg/mL as conditions providing either more compliant or stiffer 3D matrices (Heck et al., 2012; Petrie et al., 2012; Wolf et al., 2013). Neither softening nor stiffening of the matrix rescued pseudopod defects induced by SLAIN2 depletion that we observed in 2-mg/mL collagen I cultures (Figure 1J). In fact, stiffening significantly reduced pseudopod elongation in control cells (Figure 1J), possibly by activating Rho-dependent contractility (Heck et al., 2012) or providing excessive adhesion ligand.

The loss of pseudopods in SLAIN2-depleted cells correlated with strong suppression of invasive properties (Figures 1K and 1L; Movie S2). Importantly, SLAIN2-depleted cells were also unable to extend protrusions when cultured on top of a soft collagen matrix (Figures 1M, S2E, and S2F); however, despite their small size, the 2D motility of these cells was not impaired

(B and C) Western blot analysis of SLAIN2 depletion by two independent siRNAs (#1 and #2) compared with control siRNA (CT) in MDA-MB-231 and HT-1080 cells (B), and doxycycline-induced expression (dox) of the TagRFP-T-tagged dominant negative SLAIN2 mutant (SL2-N) in MDA-MB-231 cells (MDA-MB-231-SL2-N<sup>dox</sup>) (C).

(D) S-phase progression and cell division assessed by 5-ethynyl-2'-deoxyuridine (EdU) incorporation, expressed in percentage, and mitotic index in MDA-MB-231 cells treated as in (B) and (C).

(E) Changes in MT dynamics in MDA-MB-231 cells treated as in (B) and (C) and illustrated by live fluorescence images and kymographs of EB3-GFP.

(F and G) MT network in 2D- and 3D-grown MDA-MB-231 cells treated as in (B) and (C); immunofluorescence staining of  $\alpha$ -tubulin and cell outline (gray line).

(H and I) Effect of SLAIN2 inactivation on invasive cell morphology of 3D-grown cells (H) and corresponding quantification of cell elongation (I); EMT-hTMECs were transduced with the empty vector or TagRFP-T-tagged dominant negative SLAIN2-N.

(J) Quantification of SLAIN2-depleted MDA-MB-231 cell elongation in collagen I (C1) gels of different concentrations.

(K and L) Migration speed (K) and maximum invasion distance (L) of 3D-cultured cells treated as in (B) and (C).

(M) Comparison of cell morphology on 2D stiff matrix (collagen I-coated glass), on top of 2D soft matrix (2 mg/mL collagen I gel) or inside 3D soft matrix (2 mg/mL collagen I gel) using phase-contrast imaging.

Bar plots are presented as mean  $\pm$  SEM. Red line denotes the mean. In all plots, \*\*\*p < 0.001, Mann-Whitney U test; ns, no significant difference with control. See also Figures S1 and S2; Movies S1 and S2.



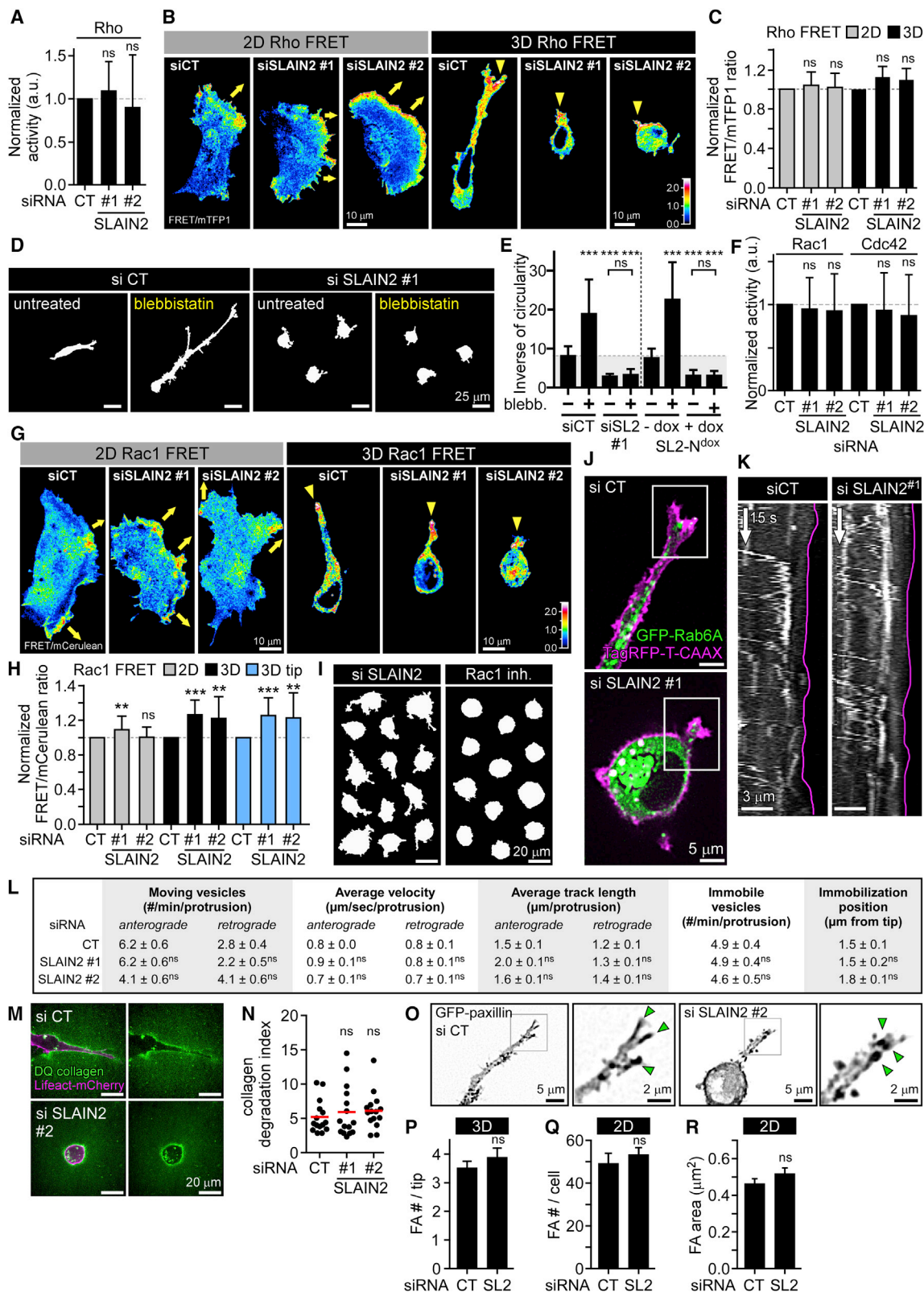


**Figure 2. Effect of SLAIN2 Inactivation in Rho GTPase Activity, Exocytotic Transport, Collagenolysis, and Focal Adhesions**

(A) Rho activation assay in control and SLAIN2-depleted cells. Error bars denote SD.

(B and C) Ratiometric representation (B) and measurement (C) of Rho biosensor activation from FRET imaging 2D- and 3D-grown cells depleted for SLAIN2. Yellow arrows, migration direction in 2D; yellow arrowheads, pseudopod tip-localized active Rho. Error bars denote SEM.

(legend continued on next page)

compared with control cells (Figures S2G and S2H). This indicates that SLAIN2 is required for cell elongation in soft environments independently of their dimensionality, but is only essential for motility in the 3D situation. Depletion of ch-TOG had the same effects as SLAIN2 inactivation on interphase cell morphology in soft 3D matrices and similarly suppressed invasiveness (Figures S2I–S2L). These results show that the SLAIN2/ch-TOG axis determines pseudopod elongation in a soft environment without affecting MT network integrity, and this function is essential for mesenchymal motility of cells embedded in 3D matrices.

### SLAIN2 Depletion Does Not Impair the Activity of Rho GTPases, Exocytotic Transport, Collagenolysis, or Adhesion Formation

MT disassembly increases cell contractility by upregulating Rho and myosin II, and reduces cell protrusion by downregulating Rac1 (Etienne-Manneville, 2013). However, using biochemical and Förster resonance energy transfer (FRET) sensor-based analysis in 2D and 3D cultures, we found that after SLAIN2 knockdown, Rho activity was not upregulated and localized normally at the leading cell edges in 2D and cell protrusions in 3D (Figures 2A–2C). Furthermore, although myosin II inhibition induced strong elongation of control cells in 3D, it completely failed to rescue formation of invasive pseudopods after SLAIN2 inactivation (Figures 2D and 2E). This indicates that Rho- and myosin II-dependent contraction did not cause the elongation defects in SLAIN2-depleted cells. The overall activities of Rac1 and Cdc42 were unchanged, and FRET biosensor imaging showed that Rac1 activity was neither reduced nor mislocalized in SLAIN2-depleted cells (Figures 2F–2H). In fact, Rac1 inhibition blocked cell elongation in 3D but also caused the loss of small protrusions, while these could still be observed in SLAIN2-depleted cells (Figure 2I). Thus Rac1 downregulation was not responsible for defects in protrusion elongation caused by SLAIN2 inactivation.

Next, we assessed MT-based transport in SLAIN2-depleted cells by imaging in 3D cultures the trafficking of exocytotic vesicles marked with GFP-Rab6A (Figures 2J and 2K; Movie S3). We found that vesicle direction, speed, track length, and tip targeting in pseudopods were not affected by SLAIN2 inactivation (Figures 2K–2L and Movie S3). This is consistent with the presence of morphologically normal MT network in these conditions (Figures 1F and 1G). In agreement with normal exocytotic trafficking, we also found no impairment of collagenolysis (Figures

2M and 2N). Furthermore, using GFP-paxillin imaging in 3D cultures as previously described (Gierke and Wittmann, 2012; Harunaga and Yamada, 2011; Kubow et al., 2013), we found no evidence of focal adhesion impairment in SLAIN2-depleted cells in either 3D or 2D cultures (Figures 2O–2R). We conclude that Rho GTPase activity, vesicle transport, matrix degradation, and focal adhesions were not affected in a way that could explain cell elongation defects in soft matrix-grown SLAIN2-deficient cells.

### SLAIN2 Promotes MT-Dependent Membrane Deformation

To test a more mechanical explanation for the SLAIN2 phenotype in 3D, we investigated whether MTs are subjected to compressive forces at pseudopod cortex. We found that growing MT ends were in very close contact with invasive pseudopod tips (Figures 3A–3C). Interestingly, EB3-GFP comets persisted much longer at the tips of pseudopods of cells grown in soft 3D matrix than at the edges of lamella spreading on top of stiff 2D matrices (Figures 3B–3D and Movie S4). A similar behavior was observed for GFP-SLAIN2 comets (Figure S1I), indicating that the differences in MT dynamics at the cell cortex in 2D and 3D were not due to differential SLAIN2 recruitment. MT persistence at the cortex was specific for elongating, but not retracting pseudopods (Figures 3E and 3F). Next, we performed whole MT imaging using  $\beta$ -tubulin-GFP in extending pseudopods in 3D and observed extensive MT buckling at pseudopod tips (20/20 cells;  $2.3 \pm 0.2$  buckling events/min at the tip [ $10 \mu\text{m}$ ]), indicating that MT growth at these sites is associated with compression (Brangwynne et al., 2006) (Figure 3G and Movie S5). Importantly, protrusion tip dynamics consisted of alternating short-scale ( $3\text{--}5 \mu\text{m}$ ) lamella-based extensions and retractions, which both correlated with MT buckling (Figure 3G and Movie S5).

We next set out to examine more directly the effect of SLAIN2 inactivation on MT resistance to compression. For this, we performed F-actin depolymerization assays, in which dynamic MTs push the membrane to form thin elongated protrusions (Figure 3H). In these conditions, cell membrane deformation correlates with the ability of MTs to withstand compression mostly driven by isometric plasma membrane tension (Wang et al., 2001; Whipple et al., 2007). Upon F-actin depolymerization in control cells, long protrusions were formed. Growing MT ends gradually decelerated and stalled at protrusion tips as they

(D and E) Effects of myosin II inhibition by blebbistatin (blebb.) on invasive morphology of 3D-grown cells (D) and quantification of cell elongation (E). Error bars denote SEM.

(F) Rac1 and Cdc42 activation assays in SLAIN2-depleted cells. Error bars denote SD.

(G and H) Ratiometric representation (G) and measurement (H) of Rac1 biosensor activation from FRET imaging in 2D- and 3D-grown cells depleted for SLAIN2 (3D tip,  $5 \mu\text{m}$ ). Yellow arrows and arrowheads as in (B). Error bars denote SEM.

(I) Comparison of the effects of Rac1 inactivation (NSC23766 inhibitor, inh.) to SLAIN2 inactivation (siRNA) on pseudopod formation.

(J and K) Transport of exocytotic vesicles marked with GFP-Rab6A in SLAIN2-depleted cells grown in 3D and expressing the membrane marker TagRFP-T-CAAX. Fluorescence images (J) and kymographs (K) showing Rab6A vesicle localization and dynamics in 3D-grown pseudopods (purple line, pseudopod tip).

(L) Quantification of GFP-Rab6A localization and dynamics at pseudopod tips ( $5 \mu\text{m}$ ) in SLAIN2-depleted cells (#, number).

(M and N) Collagenolysis visualized by live fluorescence imaging of DQ collagen in Lifeact-mCherry expressing cells depleted for SLAIN2 and grown in 3D for 2 days (M) and corresponding quantification of collagen degradation (N). Red bar denotes the mean.

(O and P) Focal adhesion formation visualized by live fluorescence imaging of GFP-paxillin in SLAIN2-depleted cells grown in 3D (O) and corresponding quantification of focal adhesion number (FA #) in pseudopod tips (P). Green arrowheads, cell tip-localized focal adhesions; error bars denote SEM.

(Q and R) Quantification of focal adhesion number per cell (Q) and area (R) in SLAIN2-depleted cells grown on a stiff 2D matrix. Error bars denote SEM.

In all plots, \*\* $p < 0.01$  and \*\*\* $p < 0.001$ , Mann-Whitney U test. ns, no significant difference with control. See also Movie S3.

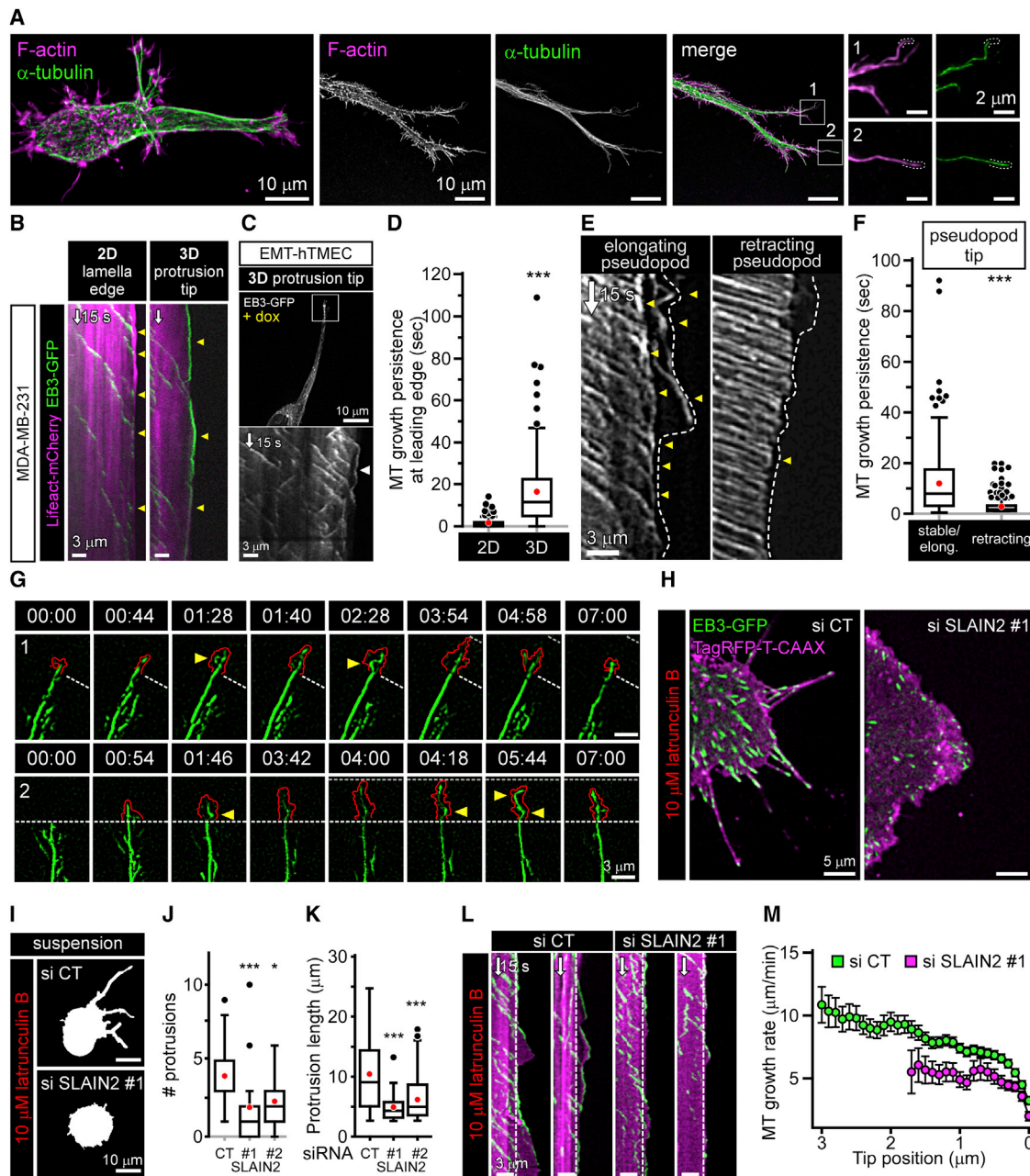


**Figure 3. MT Behavior at the Tips of Cell Protrusions**

(A) Organization of MTs in invasive pseudopods visualized by immunofluorescence staining of  $\alpha$ -tubulin (F-actin staining, phalloidin). (B and C) Persistence of MT growth at invasive pseudopod tips of mesenchymal cells grown in 3D. Fluorescence imaging and kymographs of EB3-GFP in invasive pseudopod tips of MDA-MB-231 cells (B) (compared with 2D lamella edge) and untransformed human mammary epithelial cells converted to mesenchymal phenotype by ZEB1 expression (C). Arrowheads indicate MT growth persistence at the cell edge. (D) Quantification of MT growth persistence at the leading edge (5  $\mu$ m) in 3D (pseudopod) compared with 2D (lamella). (E and F) Kymographs (E) and quantification (F) of MT growth persistence at the tips of elongating and retracting pseudopods. Arrowheads as in (B) and (C). (G) Fluorescence time-lapse images of  $\beta$ -tubulin-GFP at the tip of invasive pseudopods (1, 2). Red line, protrusion edge marked by TagRFP-T-CAAX; white dashed line, edge position at the beginning of the protrusive event; gray dashed line, edge outermost position during the protrusive event; arrowheads, MT buckling at pseudopod tips. (H–M) Cell membrane deformation by growing MT ends in SLAIN2-depleted cells treated with latrunculin B. Fluorescence images of EB3-GFP and TagRFP-T-CAAX in adherent cells (H), cell morphology (I), and quantification of protrusions formed in cells that were kept in suspension to exclude the effects of cell adhesion on protrusion formation (J and K) (#, number). Kymographs of EB3-GFP and TagRFP-T-CAAX fluorescence in cell protrusions in adherent cells (L); white dashed line, lamella edge) and deceleration profiles of growing MT ends as a function of distance to the outermost tip position (M). Error bars denote SEM. Box plots indicate the 25<sup>th</sup> percentile (bottom boundary), median (middle line), mean (red dots), 75<sup>th</sup> percentile (top boundary), nearest observations within 1.5 times the interquartile range (whiskers), and outliers (black dots). In all plots, \* $p$  < 0.05 and \*\*\* $p$  < 0.001, Mann-Whitney U test. See also [Movies S4](#) and [S5](#).



stopped elongating, as can be expected for MTs growing under load (Janson et al., 2003) (Figures 3H–3M). In SLAIN2-depleted cells, only very short and much less numerous protrusions were formed, and this correlated with slower MT growth and much quicker stalling (Figures 3H–3M). These data suggest that SLAIN2 enhances resistance of growing MTs to compression.

### MT Persistence at Pseudopod Tips and Mesenchymal Invasion Require Cooperation of SLAIN2 with Other +TIPs

Next, we set out to test whether SLAIN2/ch-TOG-driven MT growth could support pseudopod elongation independently of other +TIPs. We designed an assay based on inducible binding of two protein domains, FRB and FKBP, upon the addition of a rapamycin analog (rapalog) (Pollock et al., 2000). The ch-TOG-binding fragment SLAIN2-N (SL2-N) was fused to FRB, and an EB1-binding motif SxIP (Honnappa et al., 2009) was fused to FKBP (Figures 4A and 4B). As expected, in the absence of rapalog, SL2-N acted as a dominant negative mutant and suppressed MT growth (Figures 1 and 4B–4D), while the SxIP peptide competed with other +TIPs for the binding to EB1 (Duellberg et al., 2014; van der Vaart et al., 2011) and displaced them from MT tips (Figure 4E). Upon rapalog addition, SL2-N was recruited to MT plus ends, and processive MT growth was restored (Figures 4B–4D and Movie S6). Importantly, the localization of CLASP1 and CLIP-170 to MT plus ends was still abolished (Figure 4E), because unlike the full-length SLAIN2 (van der Vaart et al., 2011), the SL2-N-SxIP module does not bind to these proteins. Strikingly, rapalog addition rescued plasma membrane deformation by growing MTs in the absence of F-actin (Figures 4F and 4G), but not the pseudopod formation or cell invasion in soft matrices (Figures 4H–4K). We found that, in contrast to MT polymerization in the cytoplasm, MT growth persistence at pseudopod tips was not rescued by rapalog addition (Figures 4L–4N). Hence, the EB1/SLAIN2/ch-TOG complex is sufficient to drive processive growth of MTs in the cytoplasm and increases their load-bearing capacity, allowing them to push plasma membrane in the absence of F-actin. However, additional +TIPs are needed to prevent catastrophe at the actin-rich cell cortex and support pseudopod elongation in soft matrices.

### CLASP1 Is Required for the Elongation of Invasive Pseudopods and MT Growth Persistence at Their Tips

To search for factors cooperating with SLAIN2 in promoting pseudopod elongation, we tested the requirement of several +TIPs including CLASP1, CLASP2, and CLIP-170 for maintaining mesenchymal cell shape in 3D and found that CLASP2 knockdown by ~60%–70% had no effect and CLIP-170 knockdown promoted cell elongation (Figures 5A–5C). However, similar to SLAIN2 inactivation, CLASP1 knockdown abolished pseudopod elongation, 3D cell motility, and invasiveness without affecting 2D cell motility (Figures 5A–5F). Importantly, this phenotype was not due to an increase of MT catastrophe frequency in internal cell regions (Figure 5H), in agreement with our previous analysis (Mimori-Kiyosue et al., 2005). MTs in CLASP1-depleted cells could also efficiently form membrane protrusions after F-actin depolymerization (Figures 5I–5K). However, CLASP1 depletion dramatically increased catastrophe

frequency specifically at pseudopod tips (Figures 5L–5N and Movie S7). Of note, a moderate overexpression of GFP-CLASP1, which was insufficient to cause MT bundling, could not rescue pseudopod elongation defects induced by SLAIN2 depletion in soft 3D matrices (Figures 5O–5R). Together, these results suggest that mesenchymal cell elongation in soft 3D matrices requires the cooperation of CLASP1 with SLAIN2/ch-TOG to inhibit MT catastrophes in pseudopod tips.

### MT Persistence at the Tips of Invasive Pseudopods Controls Their Maintenance

We next set out to test whether MT persistence at protrusion tips is sufficient for preventing pseudopod retraction in the absence of MT growth. We used two different MTAs, vinblastine and paclitaxel, which, although they have opposing effects on MT dynamics at high concentrations, lead to a mild catastrophe induction at low doses (Mohan et al., 2013), similar to the effect of SLAIN2 inactivation (Figures 6A, S3A, and S3B; Movie S8). Importantly, in these conditions MT network, +TIP localization, and 2D cell spreading and motility were preserved (Figures 6B and S3C–S3E), as was also the case after SLAIN2 depletion.

Low-dose MTA treatments caused rapid retraction of invasive pseudopods and suppressed 3D motility (Figures 6C–6E and Movie S9), and while small pseudopods were still formed, they failed to elongate (Figure 6D and Movie S9), very similar to SLAIN2 inactivation. Increased myosin II-based contractility could not explain cell rounding in these conditions, since blebbistatin treatment failed to rescue cell elongation, again similarly to what we found in SLAIN2-depleted cells (Figure 6F). Focal adhesions and vesicle transport were maintained during cell retraction, and their perturbations could thus not explain the loss of long pseudopods (Figure S3F and Movie S10).

Strikingly, the expression of MT-stabilizing proteins MAP2C and Tau was sufficient to prevent pseudopod retraction in the absence of persistent MT growth (Figures 6G–6I and S3G). Cell motility was normal in MAP2C- and Tau-expressing cells (Figures 6J and 6K). However, after MT growth inhibition by MTA treatment, pseudopods could not remodel and 3D motility was blocked despite the fact that the invasive cell shape was maintained (Figures 6J and 6K). These data indicate that prevention of MT depolymerization at pseudopod tips is sufficient for pseudopod maintenance, but MT growth is essential for cell shape changes and, thus, cell movement in 3D.

### Interphase-Specific Induction of MT Catastrophe by SLAIN2 Inactivation Suppresses Tumor Invasion In Vivo

We next sought to test whether MT catastrophe inhibition by SLAIN2 is relevant for in vivo cell invasion. For this purpose, we orthotopically transplanted in mice luciferase-expressing MDA-MB-231 cells expressing the TagRFP-tagged dominant negative SLAIN2-N mutant under the control of doxycycline ( $n = 20$ , Figure 7A). Upon detection of palpable tumors (100 mm<sup>3</sup>), we started doxycycline administration in ten mice and monitored tumor growth and metastasis by luciferase-based bioluminescence imaging (Figure 7A). SLAIN2-N expression was efficiently induced in vivo (Figure 7A) and strikingly prevented invasive growth ( $p < 0.001$ ), resulting in expansive tumors with clearly defined borders that were confined to the mammary fat pad (Figures 7B and 7C). No significant differences were



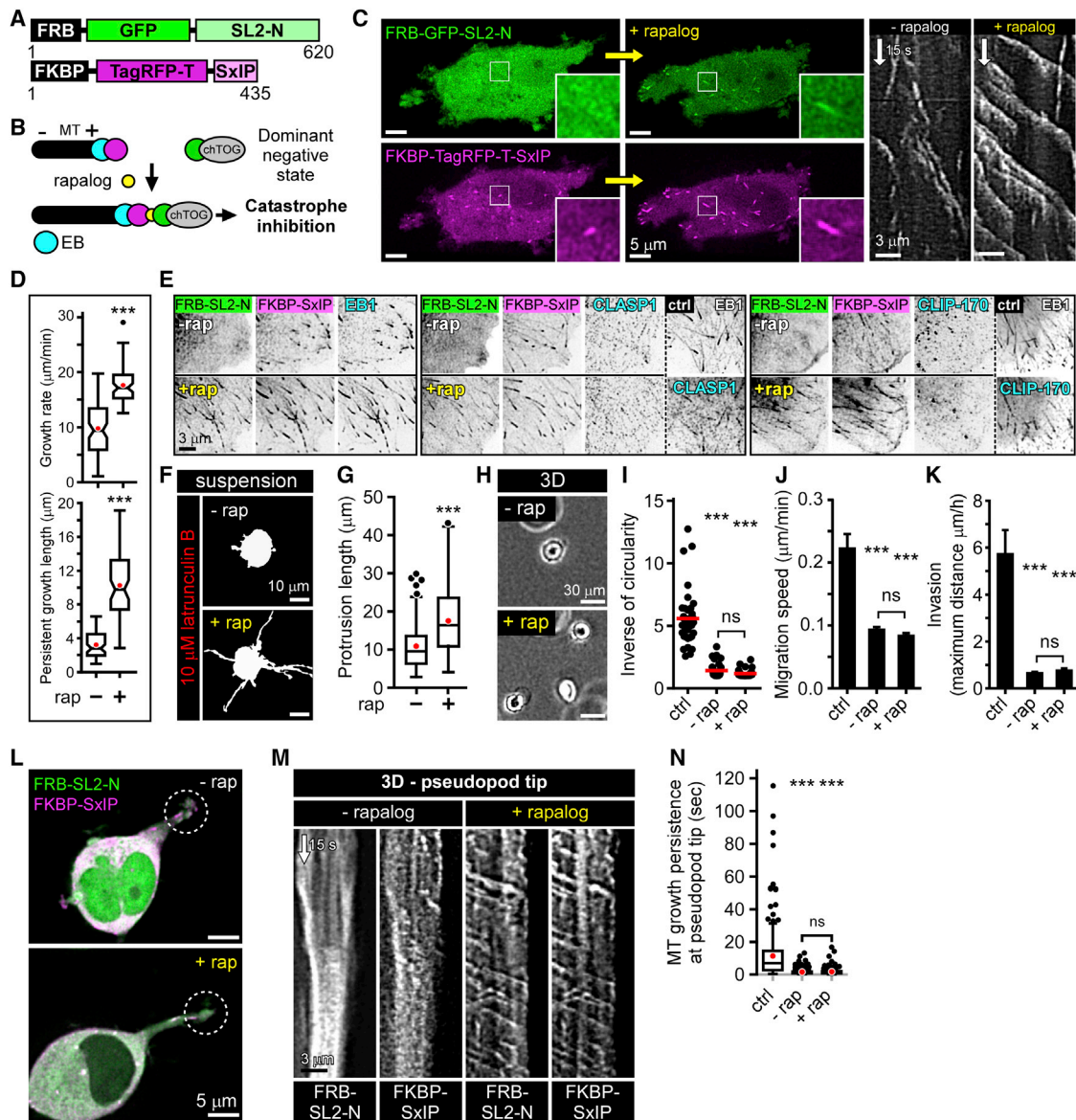


**Figure 4. SLAIN2-ch-TOG Complex Is Insufficient to Promote MT Persistence at Pseudopod Tips and Invasion**

(A and B) Fusion protein design (A) and principle (B) of the chemical dimerization-based rescue of SLAIN2-driven MT growth. Without rapalog, the SxIP peptide (purple) binds to end-binding protein (EB) (blue) at MT plus ends, while the SLAIN2-N mutant (SL2-N, green) has a dominant negative effect because it prevents ch-TOG recruitment to MT plus ends; upon the addition of rapalog (yellow), SL2-N heterodimerizes with the SxIP peptide and recruits ch-TOG to plus ends. Overexpressed SxIP peptide competes with the endogenous +TIPs for EB binding.

(C) Fluorescence images of the proteins depicted in (A), before and after rapalog addition; kymographs of FKBP-TagRFP-T-SxIP are shown on the right.

(D) MT dynamics parameters in cells treated as shown in (C), before and after rapalog (rap) addition.

(E) +TIP localization visualized by immunofluorescence staining in cells treated as shown in (C), before and after rapalog addition and compared with control (ctrl).

(F and G) Cell membrane deformation by growing MT ends in cells in suspension treated as shown in (C), with or without rapalog and treated with latrunculin B.

(H–K) Phase-contrast images (H), morphology quantification (I), migration speed (J), and invasion (K) in 3D-grown cells treated as in (C) and compared with control cells. Error bars denote SEM.

(L–N) Live fluorescence images (L) of proteins described in (A) in 3D-grown cells treated as in (C), corresponding kymographs (M), and quantification of MT growth persistence at pseudopods tips (5  $\mu$ m area) compared with control cells (N). Dashed-line circles, pseudopod tip regions used for making the kymographs.

Box plots are presented as in Figure 3; notches, 95% confidence interval of the median. In all plots, \*\*\* $p$  < 0.001, Mann-Whitney U test. ns, no significant difference with control. See also Movie S6.

observed in tumor latency ( $p$  = 0.894; Figure 7C). While we detected occasional small lung metastases in three out of ten doxycycline-treated mice, they consisted of cells that did not

express the dominant negative SLAIN2-N mutant (Figures 7C and S4A). Thus, interphase-specific induction of MT catastrophe by SLAIN2 ablation abolishes invasiveness of mesenchymal

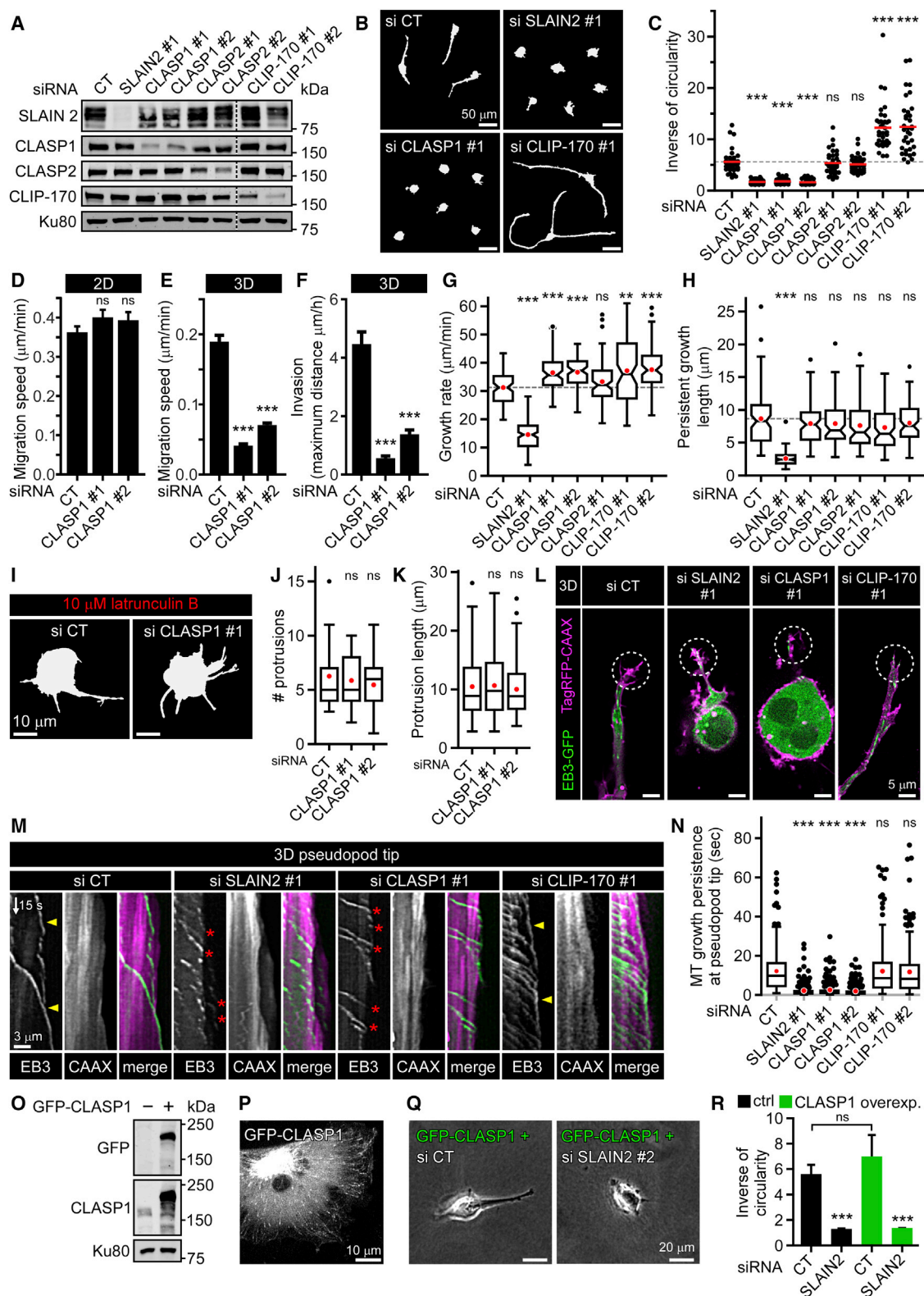


**Figure 5. CLASP1 Is Required for Mesenchymal Cell Invasion and MT Persistence at Pseudopod Tips**

(A) Western blot analysis of SLAIN2, CLASP1, CLASP2, and CLIP-170 depletion by siRNA in MDA-MB-231 cells. (B and C) Cell morphology in a 3D matrix (B) and corresponding quantification of elongation (C) in cells treated as in (A). (D–F) Migration speed in 2D (D) or 3D matrix (E) and invasion (F) in CLASP1-depleted cells. Error bars denote SEM.

(legend continued on next page)

cells in vivo and is a potent strategy to prevent mammary tumor invasion and metastatic outgrowth.

### Theoretical Model of Invasive Pseudopod Growth as a Function of MT Growth Persistence

To model how changes in MT growth persistence can affect pseudopod elongation, we performed Monte Carlo simulations based on previous studies (Dogterom and Leibler, 1993; Janson et al., 2003; Laan et al., 2008). In our model, we assumed that a compressive load, a feature that reduces growth speed and induces catastrophe (Janson et al., 2003), is applied to MTs that are longer than the average length of all MTs in the bundle (Figure 7D). We also assumed that catastrophe depends on the intrinsic resistance of individual MTs to the opposing force and the total number of MTs sharing the load (Laan et al., 2008).

The simulations showed that MT bundles can be either in “unbounded” or “bounded” growth regimes (Figure 7E), as described earlier (Dogterom and Leibler, 1993; Janson et al., 2003), the latter state being associated with the inability to support pseudopod elongation. Parametric diagrams show that a compressive force reduces the area of polymerization parameters corresponding to the unbounded growth regime (see Figure 7F); this reduction only depends on the number of MTs and their resistance to the opposing force. Consistent with experimental data, the control system remains in the unbounded state in the presence of force (blue area), whereas SLAIN2- and CLASP1-depleted systems are in the bounded regime (Figures 7F, S4B, and S4C). Moreover, this model predicts that contrarily to SLAIN2 depletion, doubling of the number of MTs in a CLASP1-depleted situation could potentially bring the system back into an unbounded state (Figure 7F). However, CLASP depletion actually tends to decrease rather than increase MT density (Mimori-Kiyosue et al., 2005), which would bring the system to a bounded regime according to our simulation. Altogether, these simulations support the idea that growth persistence of MT bundles under load is a crucial factor in soft matrix-based protrusion growth.

## DISCUSSION

Our study revealed that MT growth persistence at the cell cortex is necessary for the invasive shape and 3D motility of mesenchymal cells in vitro and in vivo. We found that an increase in MT catastrophes at pseudopod tips does not prevent pseudopod initiation but blocks pseudopod elongation, and when cells are embedded in a 3D environment this leads to a block of motility, likely because cells are unable to form distant adhesion sites to pull themselves through the matrix.

In 2D cultures the destruction of the MT network inhibits Rac1, therefore reducing protrusion, and upregulates myosin II-based contractility via Rho (Krendel et al., 2002; Waterman-Storer et al., 1999). In soft 3D matrices complete MT destruction causes pseudopod retraction, which cannot be rescued by myosin II inhibition, and it was proposed that this defect is due to Rac1 inactivation (Grinnell et al., 2003; Rhee et al., 2007). Our non-destructive approach shows that catastrophe induction by SLAIN2 or ch-TOG inactivation, or low-dose MTA treatments, causes an equally strong loss of invasive pseudopods. We demonstrate that this effect is not due to upregulated Rho and myosin II activities, downregulation of Rac1, or mislocalization of those GTPases, likely because MTs are preserved in these conditions. Cell spreading and migration in 2D, which critically depend on Rho GTPase activity and localization, are consistently unaffected by SLAIN2 inactivation. Hence, a morphogenetic function of MTs in soft matrices relies on a specific aspect of their dynamics that is mechanistically distinct from Rho GTPase regulation.

Focal adhesions control cell shape, are formed in soft 3D matrices (Harunaga and Yamada, 2011), and depend on integrin trafficking and matrix proteases (Friedl and Alexander, 2011; Jacquemet et al., 2013; Stehbens and Wittmann, 2012). Previously, invasive pseudopod defects caused by EB1 depletion were linked to altered myosin II activity, MT penetration in pseudopods, focal adhesion, and vesicle trafficking (Gierke and Wittmann, 2012). This phenotype likely reflects the perturbation of multiple mechanisms controlled by the large numbers of +TIPs that depend on EB1 for MT association (Akhmanova and Steinmetz, 2015). Here, by inactivating SLAIN2 alone, we show that increasing catastrophe frequency without affecting +TIP localization, MT density at pseudopod tips, vesicle trafficking, matrix degradation, or focal adhesions is sufficient to block pseudopod-based cell invasion.

We find that invasive pseudopod tips display highly persistent growth of MTs associated with their buckling. Buckling indicates compression, possibly generated by myosin II-based actin contraction and flow (Brangwynne et al., 2006; Gupton et al., 2002; Wang et al., 2001), membrane tension (Elbaum et al., 1996; Fygenson et al., 1997a, 1997b), MT growth itself (Dogterom and Yurke, 1997), or a combination of these factors. In fact, we observed frequent short-scale retractions of pseudopod tips associated with MT buckling, and given the limited matrix adhesion in soft 3D matrices (Harunaga and Yamada, 2011), compression of the cytoskeleton is expected (Ingber, 2003).

To analyze MT resistance to compression, we examined the ability of cells to extend membrane protrusions after actin disassembly, and found that SLAIN2/ch-TOG-driven growth

(G and H) MT dynamics parameters in cells treated as in (A).

(I–K) Cell membrane deformation by growing MTs in CLASP1-depleted cells treated with latrunculin B in suspension. Cell morphology in suspension (I) and quantification of protrusion number (#) (J) and length (K).

(L–N) Live fluorescence images (L) of EB3-GFP and TagRFP-CAAX in 3D-grown cells treated as in (A), corresponding kymographs (M), and quantification of MT growth persistence at pseudopods tips (5  $\mu\text{m}$  area) (N). Dashed-line circles, pseudopod tip regions used for making kymographs. In (M), events of persistent MT growth at pseudopod tips are indicated with yellow arrowheads and MT catastrophes at pseudopod tips by red asterisks.

(O) Western blot analysis of GFP-CLASP1 overexpression compared with endogenous expression of CLASP1 in MDA-MB-231 cells.

(P) Live fluorescence image of overexpressed GFP-CLASP1 in MDA-MB-231 cells.

(Q and R) Phase-contrast images (Q) of GFP-CLASP1 overexpressing cells as in (O), depleted for SLAIN2 and grown in 3D, and corresponding morphology analysis compared with control cells (R). Error bars denote SEM.

Box plots are presented as in Figure 3. In all plots, \*\*p < 0.01 and \*\*\*p < 0.001, Mann-Whitney U test. ns, no significant difference with control. See also Movie S7.



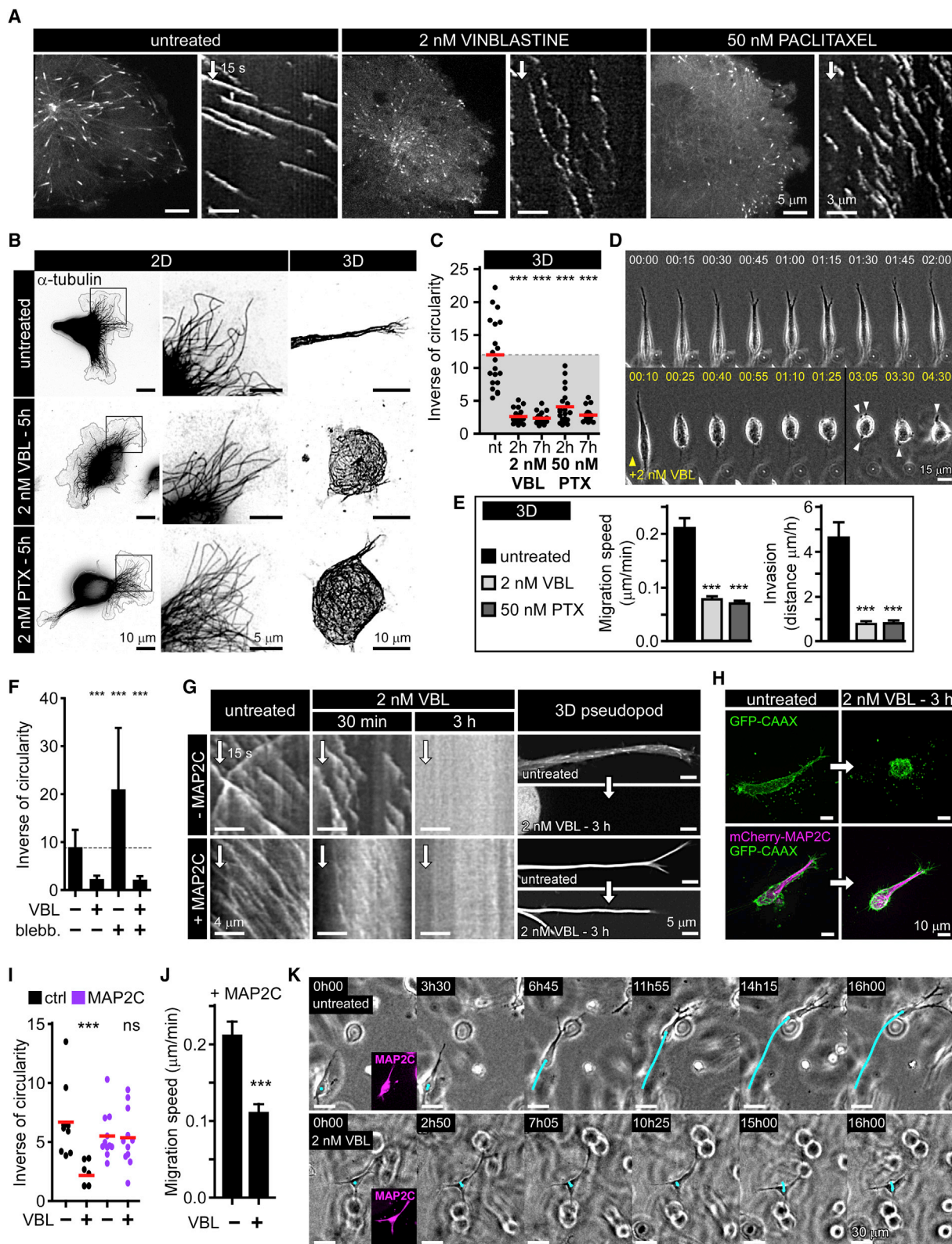


**Figure 6. Inhibition of MT Depolymerization Is Sufficient for Invasive Pseudopod Maintenance**

(A) Catastrophe induction by low doses of vinblastine (VBL) and paclitaxel (PTX) illustrated by live fluorescence images and kymographs of EB3-GFP in MDA-MB-231 cells.

(B) MT network maintenance in 2D- and 3D-grown cells treated as in (A), illustrated by immunofluorescence staining of  $\alpha$ -tubulin.

(legend continued on next page)



persistence was essential for this process while other EB1-associated +TIPs were likely dispensable. However, in the presence of actin, additional factors were necessary to prevent catastrophes, possibly due to a different biochemical environment of the actin-rich cortex or higher forces exerted at pseudopod extremities. We identified one such factor as CLASP1, which contributes to catastrophe suppression by acting specifically at pseudopod tips. CLASP1 is a well-studied MT-stabilizing protein and a rescue factor (Al-Bassam and Chang, 2011; Mimori-Kiyosue et al., 2005). CLASP1 depletion induced catastrophes only at the cell cortex, which is in line with the previously described local function of CLASPs at the leading cell edge (Akhmanova et al., 2001; Wittmann and Waterman-Storer, 2005). It is possible that CLASP1 partners such as LL5 $\beta$  or +TIPs acting in the same complexes, such as spectraplakins (Drabek et al., 2006; Lansbergen et al., 2006), also participate in regulating MT dynamics in pseudopods. Local differences between the localization and activity of CLASP1 or its partners might explain the differences in MT growth persistence between protruding and retracting pseudopods. The crosstalk between MTs and actin could also play an important role, especially as the actin organization in 2D and 3D is different, with 3D cells lacking prominent actin-based structures such as stress fibers and large lamellae. Differences in actomyosin-based retrograde flow, which can affect MT dynamics (Gupton et al., 2002; Waterman-Storer and Salmon, 1997), might explain why MTs grow more persistently at pseudopod tips in 3D than at the edges of lamella in 2D.

Interestingly, our data emphasize the fundamental difference between neurons and 3D-grown mesenchymal cells in the dependence of their shape on MT growth. SLAIN2 inactivation caused only limited defects in axon elongation (van der Vaart et al., 2011), and in fact low doses of paclitaxel can even promote axon outgrowth (Witte et al., 2008). Neurons express many stabilizing MT-associated proteins (MAPs), which can counteract neurite retraction when MT growth is perturbed. In contrast, the ability of mesenchymal cells to make long protrusions and move in 3D critically depends on dynamic MTs. Interestingly, we show that introducing neuronal MAPs makes mesenchymal cells less sensitive to retraction caused by MT growth perturbations, although processive MT growth is still needed for their 3D motility.

Together with our computational modeling, our experimental data suggest that catastrophe inhibition promotes a load-bearing role for MTs during cell elongation in soft matrix. We propose a model in which SLAIN2/ch-TOG and CLASP1, by reducing catastrophe frequency at the cortex, allow MTs

to support a part of the compression generated by cellular prestress in soft matrices (Ingber, 2003). Accordingly in mesenchymal cell invasion, while actin and matrix adhesion drive elongation, MTs can bear the load to oppose cell retraction (Figure 7G). We propose that this mechanism is important on top of or within soft matrices, but not on stiff matrices, where the substrate itself, in combination with strong cell adhesion to the matrix, can serve as a mechanical element to prevent cell retraction. In agreement with this view, perturbation of persistent MT growth on top of a soft 2D gel strongly impaired cell spreading. However, this did not inhibit cell motility because cells could essentially “roll over,” even though their protrusions were small. In contrast, within a 3D gel the inability to elongate pseudopods inhibited the capacity of cells to form distant adhesions, making them immotile. Taken together, these data indicate that the importance of MT dynamics for making cell protrusions depends on matrix stiffness, while the importance of long protrusions for cell movement depends on substrate dimensionality. While our data support a “mechanical” model of MT-dependent control of cell shape, we cannot rule out potential alternative pathways involving either signaling or trafficking, which might connect MT growth persistence to pseudopod elongation in soft matrices.

Interphase rather than mitosis has been proposed to be the major target of MTAs in cancer therapy (Komlodi-Pasztor et al., 2011; Mitchison, 2012). In parallel, targeting interphase cell migration could be a very potent anti-metastatic strategy in invasive cancers (Cheung and Ewald, 2014; Palmer et al., 2011). Our finding that SLAIN2 inactivation in cancer cells inhibits tumor invasion and metastasis in an interphase-specific manner has major implications for cancer therapeutics. It supports the idea that anti-metastatic action of MTAs relates to their anti-migratory effects in interphase cells. It also suggests that SLAIN2 itself is a potential target for metastatic cancer treatment that can be further studied using the tools developed in this study.

## EXPERIMENTAL PROCEDURES

The description of the details of the constructs, small interfering RNAs (siRNAs), cell culture, cell transfection, lentiviral infection methods, cell staining, tissue immunohistochemistry, image analysis, and modeling can be found in [Supplemental Experimental Procedures](#).

### Cell Lines and 3D Culture

MDA-MB-231 cells were obtained from J. Martens (Erasmus MC Rotterdam, the Netherlands) and cultured respectively in DMEM supplemented with 10% fetal calf serum (FCS). HT-1080 cells were a gift of K. Wolf (Radboud

(C) Quantification of invasive morphology of 3D-grown cells treated as in (A).

(D) Phase-contrast images from time-lapse recording of mesenchymal cells migrating in a 3D matrix and treated when indicated by vinblastine as in (A). Arrowheads indicate the formation of small pseudopods that fail to elongate.

(E) Migration speed and invasion of mesenchymal cells grown in 3D and treated as in (A).

(F) Effect of myosin II inhibition (blebb., blebbistatin) on invasive morphology of cells treated as in (A).

(G) Effect of MAP2C expression on the maintenance of invasive pseudopods when MT growth persistence is attenuated. Kymographs show EB3-GFP dynamics in cells treated as indicated, and panels on the right show invasive pseudopods before and after treatment; in +MAP2C condition; images are mCherry-MAP2C fluorescence.

(H and I) Invasive morphology (H) and its quantification (I) in 3D-grown mesenchymal cells before and after attenuation of persistent MT growth by vinblastine as in (A), with or without MAP2C expression.

(J and K) 3D migration speed (J) and invasive behavior (K) of MAP2C-expressing cells treated as in (A).

Bar plots are presented as mean  $\pm$  SEM. Red line denotes the mean. In all plots, \*\*\* $p < 0.001$ , Mann-Whitney U test. ns, no significant difference with control. See also [Figure S3](#); [Movies S8](#), [S9](#), and [S10](#).

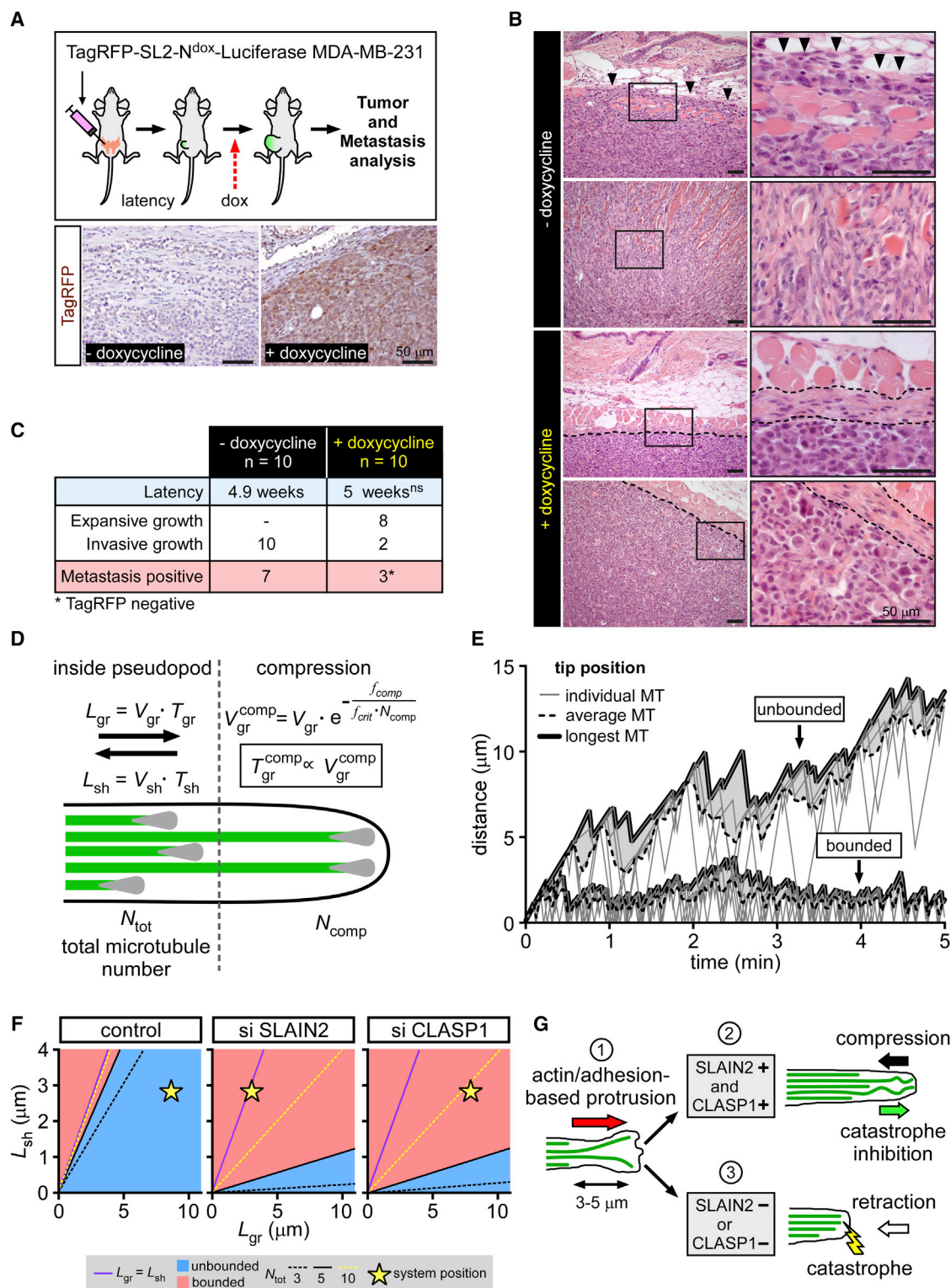


**Figure 7. Interphase-Specific Attenuation of SLAIN2/ch-TOG-Driven MT Growth Suppresses Tumor Invasion In Mice**

(A) Luciferase-expressing MDA-MB-231 cells carrying a doxycycline-controlled expression construct for TagRFP-tagged dominant negative SLAIN2 mutant (SL2-N) were orthotopically transplanted into recipient mice. When tumor volume exceeded 1,000 mm<sup>3</sup> or upon detection of metastases by bioluminescence imaging the mice were euthanized, and tumors and metastases were further analyzed by anatomic pathology evaluation. Bottom panel, immunohistochemical staining of TagRFP in primary tumors from mice treated or untreated with doxycycline.

(legend continued on next page)

University Nijmegen, the Netherlands) and were cultured in DMEM supplemented with 10% FCS. Clonal versions of the original MDA-MB-231 cell line were selected according to their high invasiveness in 3D matrix. Primary human mammary epithelial cells (HMECs) were purchased from Lonza and cultured in MEGM (MEBM and supplement). HEK293T cells were cultured in DMEM supplemented with 10% FCS. hTERT-immortalized HMECs (hTMECs) were generated by viral transduction of hTERT in HMECs using the pBABE-hygro-hTERT plasmid and 50  $\mu$ g/mL hygromycin selection.

3D cultures of MDA-MB-231, HT-1080, and doxycycline-treated EMT-hTMEC cells were set up by cell suspension seeding in 2 mg/mL rat tail collagen I gels neutralized according to manufacturer protocol; for stiffness-related experiments, collagen concentration was changed as mentioned. EMT-hTMEC 3D culture without doxycycline was performed in Matrigel or a mix of Matrigel with neutralized collagen I, and growth-arrested acini were obtained within 10–20 days as previously described (Seton-Rogers et al., 2004). 2D cultures were set up either on non-coated or collagen I-coated coverslips (12 M HCl wash, poly-D-lysine coating in borate buffer [1.24 g of boric acid, 1.9 g of sodium tetraborate, 400 mL of milliQ water, pH 8.5] and 500  $\mu$ g/mL collagen I coating).

### Live-Cell Imaging

Fluorescence imaging of 2D and 3D live cultures was performed on a Nikon spinning disk-based confocal imaging station described in Supplemental Experimental Procedures using a stage-top incubator INUBG2E-ZILCS (Tokai Hit) for 37°C/5% CO<sub>2</sub> incubation and 37°C lens heating. Simultaneous two-color imaging was performed using the DV2 two-channel simultaneous-imaging system (Photometrics) equipped with the dichroic filter 565dcxr (Chroma). 2D imaging was performed using Nikon Apo TIRF 100 $\times$  numerical aperture (NA) 1.49 oil, Plan Apo VC 60 $\times$  NA 1.4, or Plan Fluor 40 $\times$  NA 1.3 objectives. 3D imaging was performed using a Nikon Apo LWD  $\lambda$ S 40 $\times$  NA 1.15 water-immersion objective eventually combined with the Nikon Ti intermediate 1.5 $\times$  magnification lens.

### Mouse Experiments

All animal experiments were approved by the Utrecht University Animal Experimental Committee (DEC-ABC no. 2014.III.08.075). The fourth (inguinal) mammary gland from female RAG2<sup>-/-</sup>;IL-2R $\gamma$ C<sup>-/-</sup> immunodeficient mice (Gimeno et al., 2004) was exposed and approximately 10<sup>6</sup> MDA-MB-231 cells expressing luciferase and carrying doxycycline-inducible expression of SLAIN2-N were injected using a 50- $\mu$ L Hamilton syringe. Buprenorphine (Temgesic), 100  $\mu$ L (0.03 mg/mL) was injected subcutaneously as analgesic treatment. Tumor growth was measured using a digital caliper (Mitutoyo) on a weekly basis. Upon development of palpable tumors, mice were switched from a standard diet to doxycycline-containing chow (A153D00201; Sniff) for the remainder of the experiment. Luciferase-based bioluminescence of primary tumor and metastases was monitored as previously described (Schackmann et al., 2011). Mice were euthanized when tumor volume exceeded 1,000 mm<sup>3</sup> or when bioluminescence imaging revealed metastases.

### SUPPLEMENTAL INFORMATION

Supplemental Information includes Supplemental Experimental Procedures, four figures, and ten movies and can be found with this article online at <http://dx.doi.org/10.1016/j.devcel.2016.11.009>.

### AUTHOR CONTRIBUTIONS

B.P.B., I.N., M.D., P.W.B.D., and A.A. designed the experiments and wrote the paper. B.P.B., I.N., Y.-C. A., M.v.A., and N.D.t.H. conducted the experiments and analyzed the data. E.A.K. analyzed data in Figure 3M. B.P.B., E.A.K., and M.D. conceived the theoretical model; E.A.K. developed the model and carried out the computer-based simulations. L.H. generated reagents.

### ACKNOWLEDGMENTS

We are grateful to Dr. I. Grigoriev for assistance with microscopy; J. van der Beek and J. Bertram for help with cloning and 3D cultures; L. Kapitein and G. Koenderink for critically reading the manuscript; and R. Weinberg, M. Sixt, R. Wedlich-Söldner, Y. Mimori-Kiyosue, K. Jiang, L. Cassimeris, I. Barde, D. Trono, J. E. Mertz, O. Pertz, S. Vogel, M. Davidson, D. Piston, P. Schätzle, C. Hoogenraad, E. Bindels, E. Soler, J. Martens, S. Royle, and K. Wolf for the gift of reagents. This work was supported by the Netherlands Organisation for Scientific Research (NWO) through an ALW-VICI grant 865.08.002 and ALW Open Program grant 822.02.002 to A.A., European Research Council (ERC) Synergy Grant 609822 to M.D. and A.A., Marie Skłodowska-Curie Actions Innovative Training Network PolarNet 675407, Fondation pour la Recherche Médicale and Marie Curie International Intra-European Fellowship to B.P.B., NWO/ZonMW-VICI 016.096.318 to P.W.D., and Foundation Vrienden UMC Utrecht (11.081), the Dutch Cancer Society (KWF-UU-2011-5230 and KWF-UU-2014-7201), and National Cancer Institute grant CA181838 to L.H.

Received: June 9, 2016

Revised: September 27, 2016

Accepted: November 10, 2016

Published: December 8, 2016

### REFERENCES

- Akhmanova, A., and Steinmetz, M.O. (2015). Control of microtubule organization and dynamics: two ends in the limelight. *Nat. Rev. Mol. Cell Biol.* **16**, 711–726.
- Akhmanova, A., Hoogenraad, C.C., Drabek, K., Stepanova, T., Dortland, B., Verkerk, T., Vermeulen, W., Burgering, B.M., De Zeeuw, C.I., Grosveld, F., and Galjart, N. (2001). Clasps are CLIP-115 and -170 associating proteins involved in the regional regulation of microtubule dynamics in motile fibroblasts. *Cell* **104**, 923–935.

(B) H&E staining in primary tumors from the mice transplanted and treated as explained in (A). Note that highly invasive control cells infiltrate the striated subcutaneous muscle layer (arrowheads). Doxycycline-treated mice: in the left panels, dotted line indicates primary tumor margin; in the right panels, dotted lines indicate clear and intact demarcation of the dermal/epidermal basement membrane.

(C) Latency, primary tumor growth classification, and metastasis evaluation in mice transplanted and treated as explained in (A). ns, not significant (t test).

(D) Schematic representation of the model. MT dynamic instability parameters are different for MTs deep inside pseudopods and those compressed against the extending edge. See Supplemental Experimental Procedures for details.

(E) Examples of simulations corresponding to the “bounded” (bottom) and “unbounded” (top) growth. Thick solid lines depict the growing edge of the pseudopod defined by the longest MT. Gray area marks the distance between the edge and the average MT length. Thin gray lines correspond to individual MTs.

(F) Parametric diagrams corresponding to the control condition, SLAIN2 depletion, and CLASP depletion. For x axis  $L_{gr} = V_{gr} \cdot T_{gr}$  and for y axis  $L_{sh} = V_{sh} \cdot T_{sh}$ . Purple line marks a boundary between the “bounded” and “unbounded” growth in case of unconstrained MT growth. Blue areas correspond to the “unbounded” growth regime in the presence of the cell cortex for  $N_{tot} = 5$ . Dashed lines mark transition boundaries for the  $N_{tot} = 3$  (black) and  $N_{tot} = 10$  (yellow). Star indicates state of the system in each condition.

(G) Proposed model for the role of MT growth persistence in pseudopod elongation in soft matrix. The leading edge is formed by the tip of a pseudopod that elongates via a succession of short small-amplitude protrusions driven by actin and matrix adhesion (1). When both SLAIN2 and CLASP1 are present (2), growing MTs persist at the pseudopod tip, where they resist compression and counteract retraction. Pseudopod tip is stabilized and can undergo a new cycle of protrusion/stabilization. When SLAIN2 or CLASP1 are inactivated (3), MTs engaged in the newly formed protrusion undergo catastrophe due to unknown factors and are unable to counteract retraction. The pseudopod fails to maintain the newly formed protrusion and retracts.

See also Figure S4.



- Al-Bassam, J., and Chang, F. (2011). Regulation of microtubule dynamics by TOG-domain proteins XMAP215/Dis1 and CLASP. *Trends Cell Biol.* 21, 604–614.
- Brangwynne, C.P., MacKintosh, F.C., Kumar, S., Geisse, N.A., Talbot, J., Mahadevan, L., Parker, K.K., Ingber, D.E., and Weitz, D.A. (2006). Microtubules can bear enhanced compressive loads in living cells because of lateral reinforcement. *J. Cell Biol.* 173, 733–741.
- Chaffer, C.L., and Weinberg, R.A. (2011). A perspective on cancer cell metastasis. *Science* 331, 1559–1564.
- Cheung, K.J., and Ewald, A.J. (2014). Invasive leader cells: metastatic oncotarget. *Oncotarget* 5, 1390–1391.
- Cheung, K.J., Gabrielson, E., Werb, Z., and Ewald, A.J. (2013). Collective invasion in breast cancer requires a conserved basal epithelial program. *Cell* 155, 1639–1651.
- Clark, A.G., and Vignjevic, D.M. (2015). Modes of cancer cell invasion and the role of the microenvironment. *Curr. Opin. Cell Biol.* 36, 13–22.
- Dennerll, T.J., Joshi, H.C., Steel, V.L., Buxbaum, R.E., and Heidemann, S.R. (1988). Tension and compression in the cytoskeleton of PC-12 neurites. II: quantitative measurements. *J. Cell Biol.* 107, 665–674.
- Dogterom, M., and Leibler, S. (1993). Physical aspects of the growth and regulation of microtubule structures. *Phys. Rev. Lett.* 70, 1347–1350.
- Dogterom, M., and Yurke, B. (1997). Measurement of the force-velocity relation for growing microtubules. *Science* 278, 856–860.
- Drabek, K., van, H.M., Stepanova, T., Draegestein, K., van, H.R., Sayas, C.L., Akhmanova, A., Ten, H.T., Smits, R., Fodde, R., et al. (2006). Role of CLASP2 in microtubule stabilization and the regulation of persistent motility. *Curr. Biol.* 16, 2259–2264.
- Duellberg, C., Trokter, M., Jha, R., Sen, I., Steinmetz, M.O., and Surrey, T. (2014). Reconstitution of a hierarchical +TIP interaction network controlling microtubule end tracking of dynein. *Nat. Cell Biol.* 16, 804–811.
- Elbaum, M., Fygenson, D.K., and Libchaber, A. (1996). Buckling microtubules in vesicles. *Phys. Rev. Lett.* 76, 4078–4081.
- Etienne-Manneville, S. (2013). Microtubules in cell migration. *Annu. Rev. Cell Dev. Biol.* 29, 471–499.
- Friedl, P., and Alexander, S. (2011). Cancer invasion and the microenvironment: plasticity and reciprocity. *Cell* 147, 992–1009.
- Friedl, P., and Gilmour, D. (2009). Collective cell migration in morphogenesis, regeneration and cancer. *Nat. Rev. Mol. Cell Biol.* 10, 445–457.
- Fygenson, D.K., Elbaum, M., Shraiman, B., and Libchaber, A. (1997a). Microtubules and vesicles under controlled tension. *Phys. Rev. E* 55, 850–859.
- Fygenson, D.K., Marko, J.F., and Libchaber, A. (1997b). Mechanics of microtubule-based membrane extension. *Phys. Rev. Lett.* 79, 4497–4500.
- Gierke, S., and Wittmann, T. (2012). EB1-recruited microtubule +TIP complexes coordinate protrusion dynamics during 3D epithelial remodeling. *Curr. Biol.* 22, 753–762.
- Gimeno, R., Weijer, K., Voordouw, A., Uittenbogaart, C.H., Legrand, N., Alves, N.L., Wijnands, E., Blom, B., and Spits, H. (2004). Monitoring the effect of gene silencing by RNA interference in human CD34+ cells injected into newborn RAG2-/- gammaC-/- mice: functional inactivation of p53 in developing T cells. *Blood* 104, 3886–3893.
- Grinnell, F., and Petroll, W.M. (2010). Cell motility and mechanics in three-dimensional collagen matrices. *Annu. Rev. Cell Dev. Biol.* 26, 335–361.
- Grinnell, F., Ho, C.H., Tamariz, E., Lee, D.J., and Skuta, G. (2003). Dendritic fibroblasts in three-dimensional collagen matrices. *Mol. Biol. Cell* 14, 384–395.
- Gupton, S.L., Salmon, W.C., and Waterman-Storer, C.M. (2002). Converging populations of f-actin promote breakage of associated microtubules to spatially regulate microtubule turnover in migrating cells. *Curr. Biol.* 12, 1891–1899.
- Harunaga, J.S., and Yamada, K.M. (2011). Cell-matrix adhesions in 3D. *Matrix Biol.* 30, 363–368.
- Heck, J.N., Ponik, S.M., Garcia-Mendoza, M.G., Pehlke, C.A., Inman, D.R., Eliceiri, K.W., and Keely, P.J. (2012). Microtubules regulate GEF-H1 in response to extracellular matrix stiffness. *Mol. Biol. Cell* 23, 2583–2592.
- Honnappa, S., Gouveia, S.M., Weisbrich, A., Damberger, F.F., Bhavesh, N.S., Jawhari, H., Grigoriev, I., van Rijssel, F.J., Buey, R.M., Lawera, A., et al. (2009). An EB1-binding motif acts as a microtubule tip localization signal. *Cell* 138, 366–376.
- Ingber, D.E. (2003). Tensegrity I. Cell structure and hierarchical systems biology. *J. Cell Sci* 116, 1157–1173.
- Jacquemet, G., Humphries, M.J., and Caswell, P.T. (2013). Role of adhesion receptor trafficking in 3D cell migration. *Curr. Opin. Cell Biol.* 25, 627–632.
- Janson, M.E., de Dood, M.E., and Dogterom, M. (2003). Dynamic instability of microtubules is regulated by force. *J. Cell Biol.* 161, 1029–1034.
- Kikuchi, K., and Takahashi, K. (2008). WAVE2- and microtubule-dependent formation of long protrusions and invasion of cancer cells cultured on three-dimensional extracellular matrices. *Cancer Sci.* 99, 2252–2259.
- Komlodi-Pasztor, E., Sackett, D., Wilkerson, J., and Fojo, T. (2011). Mitosis is not a key target of microtubule agents in patient tumors. *Nat. Rev. Clin. Oncol.* 8, 244–250.
- Krendel, M., Zenke, F.T., and Bokoch, G.M. (2002). Nucleotide exchange factor GEF-H1 mediates cross-talk between microtubules and the actin cytoskeleton. *Nat. Cell Biol.* 4, 294–301.
- Kubow, K.E., Conrad, S.K., and Horwitz, A.R. (2013). Matrix microarchitecture and myosin II determine adhesion in 3D matrices. *Curr. Biol.* 23, 1607–1619.
- Kutys, M.L., and Yamada, K.M. (2014). An extracellular-matrix-specific GEF-GAP interaction regulates Rho GTPase crosstalk for 3D collagen migration. *Nat. Cell Biol.* 16, 909–917.
- Laan, L., Husson, J., Munteanu, E.L., Kerssemakers, J.W., and Dogterom, M. (2008). Force-generation and dynamic instability of microtubule bundles. *Proc. Natl. Acad. Sci. USA* 105, 8920–8925.
- Lam, P.Y., and Huttenlocher, A. (2013). Interstitial leukocyte migration in vivo. *Curr. Opin. Cell Biol.* 25, 650–658.
- Lansbergen, G., Grigoriev, I., Mimori-Kiyosue, Y., Ohtsuka, T., Higa, S., Kitajima, I., Demmers, J., Galjart, N., Houtsmuller, A.B., Grosveld, F., and Akhmanova, A. (2006). CLASPs attach microtubule plus ends to the cell cortex through a complex with LL5beta. *Dev. Cell* 11, 21–32.
- Lee, M.H., Wu, P.H., Gilkes, D., Aifuwa, I., and Wirtz, D. (2015). Normal mammary epithelial cells promote carcinoma basement membrane invasion by inducing microtubule-rich protrusions. *Oncotarget* 6, 32634–32645.
- Martins, G.G., and Kolega, J. (2012). A role for microtubules in endothelial cell protrusion in three-dimensional matrices. *Biol. Cell* 104, 271–286.
- Matrone, M.A., Whipple, R.A., Thompson, K., Cho, E.H., Vitolo, M.I., Balzer, E.M., Yoon, J.R., Ioffe, O.B., Tuttle, K.C., Tan, M., and Martin, S.S. (2010). Metastatic breast tumors express increased tau, which promotes microtubule formation and the reattachment of detached breast tumor cells. *Oncogene* 29, 3217–3227.
- Mimori-Kiyosue, Y., Grigoriev, I., Lansbergen, G., Sasaki, H., Matsui, C., Severin, F., Galjart, N., Grosveld, F., Vorobjev, I., Tsukita, S., and Akhmanova, A. (2005). CLASP1 and CLASP2 bind to EB1 and regulate microtubule plus-end dynamics at the cell cortex. *J. Cell Biol.* 168, 141–153.
- Mitchison, T.J. (2012). The proliferation rate paradox in antimitotic chemotherapy. *Mol. Biol. Cell* 23, 1–6.
- Mohan, R., Katrukha, E.A., Doodhi, H., Smal, I., Meijering, E., Kapitein, L.C., Steinmetz, M.O., and Akhmanova, A. (2013). End-binding proteins sensitize microtubules to the action of microtubule-targeting agents. *Proc. Natl. Acad. Sci. USA* 110, 8900–8905.
- Nakaya, Y., and Sheng, G. (2008). Epithelial to mesenchymal transition during gastrulation: an embryological view. *Dev. Growth Differ.* 50, 755–766.
- Oyanagi, J., Ogawa, T., Sato, H., Higashi, S., and Miyazaki, K. (2012). Epithelial-mesenchymal transition stimulates human cancer cells to extend microtubule-based invasive protrusions and suppresses cell growth in collagen gel. *PLoS One* 7, e53209.
- Palmer, T.D., Ashby, W.J., Lewis, J.D., and Zijlstra, A. (2011). Targeting tumor cell motility to prevent metastasis. *Adv. Drug Deliv. Rev.* 63, 568–581.
- Petrie, R.J., and Yamada, K.M. (2015). Fibroblasts lead the way: a unified view of 3D cell motility. *Trends Cell Biol.* 25, 666–674.



- Petrie, R.J., Gavara, N., Chadwick, R.S., and Yamada, K.M. (2012). Nonpolarized signaling reveals two distinct modes of 3D cell migration. *J. Cell Biol.* **197**, 439–455.
- Pollock, R., Issner, R., Zoller, K., Natesan, S., Rivera, V.M., and Clackson, T. (2000). Delivery of a stringent dimerizer-regulated gene expression system in a single retroviral vector. *Proc. Natl. Acad. Sci. USA* **97**, 13221–13226.
- Pourroy, B., Honore, S., Pasquier, E., Bourgarel-Rey, V., Kruczynski, A., Briand, C., and Braguer, D. (2006). Antiangiogenic concentrations of vinflunine increase the interphase microtubule dynamics and decrease the motility of endothelial cells. *Cancer Res.* **66**, 3256–3263.
- Rhee, S., Jiang, H., Ho, C.H., and Grinnell, F. (2007). Microtubule function in fibroblast spreading is modulated according to the tension state of cell-matrix interactions. *Proc. Natl. Acad. Sci. USA* **104**, 5425–5430.
- Sahai, E., and Marshall, C.J. (2003). Differing modes of tumour cell invasion have distinct requirements for Rho/ROCK signalling and extracellular proteolysis. *Nat. Cell Biol.* **5**, 711–719.
- Sanz-Moreno, V., and Marshall, C.J. (2010). The plasticity of cytoskeletal dynamics underlying neoplastic cell migration. *Curr. Opin. Cell Biol.* **22**, 690–696.
- Schackmann, R.C., van, A.M., Haarhuis, J.H., Vlug, E.J., Halim, V.A., Roodhart, J.M., Vermaat, J.S., Voest, E.E., van der Groep, P., van Diest, P.J., et al. (2011). Cytosolic p120-catenin regulates growth of metastatic lobular carcinoma through Rock1-mediated anoikis resistance. *J. Clin. Invest.* **121**, 3176–3188.
- Seton-Rogers, S.E., Lu, Y., Hines, L.M., Koundinya, M., LaBaer, J., Muthuswamy, S.K., and Brugge, J.S. (2004). Cooperation of the ErbB2 receptor and transforming growth factor beta in induction of migration and invasion in mammary epithelial cells. *Proc. Natl. Acad. Sci. USA* **101**, 1257–1262.
- Stehbens, S., and Wittmann, T. (2012). Targeting and transport: how microtubules control focal adhesion dynamics. *J. Cell Biol.* **198**, 481–489.
- Tomasek, J.J., and Hay, E.D. (1984). Analysis of the role of microfilaments and microtubules in acquisition of bipolarity and elongation of fibroblasts in hydrated collagen gels. *J. Cell Biol.* **99**, 536–549.
- Tran, T.A., Gillet, L., Roger, S., Besson, P., White, E., and Le Guennec, J.Y. (2009). Non-anti-mitotic concentrations of taxol reduce breast cancer cell invasiveness. *Biochem. Biophys. Res. Commun.* **379**, 304–308.
- van der Vaart, B., Manatschal, C., Grigoriev, I., Olieric, V., Gouveia, S.M., Bjelic, S., Demmers, J., Vorobjev, I., Hoogenraad, C.C., Steinmetz, M.O., and Akhmanova, A. (2011). SLAIN2 links microtubule plus end-tracking proteins and controls microtubule growth in interphase. *J. Cell Biol.* **193**, 1083–1099.
- Wang, N., Naruse, K., Stamenovic, D., Fredberg, J.J., Mijailovich, S.M., Tolic-Norrelykke, I.M., Polte, T., Mannix, R., and Ingber, D.E. (2001). Mechanical behavior in living cells consistent with the tensegrity model. *Proc. Natl. Acad. Sci. USA* **98**, 7765–7770.
- Waterman-Storer, C.M., and Salmon, E.D. (1997). Actomyosin-based retrograde flow of microtubules in the lamella of migrating epithelial cells influences microtubule dynamic instability and turnover and is associated with microtubule breakage and treadmilling. *J. Cell Biol.* **139**, 417–434.
- Waterman-Storer, C.M., Worthylake, R.A., Liu, B.P., Burridge, K., and Salmon, E.D. (1999). Microtubule growth activates Rac1 to promote lamellipodial protrusion in fibroblasts. *Nat. Cell Biol.* **1**, 45–50.
- Whipple, R.A., Cheung, A.M., and Martin, S.S. (2007). Detyrosinated microtubule protrusions in suspended mammary epithelial cells promote reattachment. *Exp. Cell Res.* **313**, 1326–1336.
- Wilson, K., Lewalle, A., Fritzsche, M., Thorogate, R., Duke, T., and Charras, G. (2013). Mechanisms of leading edge protrusion in interstitial migration. *Nat. Commun.* **4**, 2896.
- Winckler, B., and Solomon, F. (1991). A role for microtubule bundles in the morphogenesis of chicken erythrocytes. *Proc. Natl. Acad. Sci. USA* **88**, 6033–6037.
- Witte, H., Neukirchen, D., and Bradke, F. (2008). Microtubule stabilization specifies initial neuronal polarization. *J. Cell Biol.* **180**, 619–632.
- Wittmann, T., and Waterman-Storer, C.M. (2005). Spatial regulation of CLASP affinity for microtubules by Rac1 and GSK3beta in migrating epithelial cells. *J. Cell Biol.* **169**, 929–939.
- Wolf, K., Te, L.M., Krause, M., Alexander, S., Te, R.J., Willis, A.L., Hoffman, R.M., Figdor, C.G., Weiss, S.J., and Friedl, P. (2013). Physical limits of cell migration: control by ECM space and nuclear deformation and tuning by proteolysis and traction force. *J. Cell Biol.* **201**, 1069–1084.
- Zhang, P., Sun, Y., and Ma, L. (2015). ZEB1: at the crossroads of epithelial-mesenchymal transition, metastasis and therapy resistance. *Cell Cycle* **14**, 481–487.